JOURNAL OF SYNCHROTRON RADIATION
ISSN 1600-5775

Observation of two-dimensional yttrium oxide nanoparticles in mealworm beetles (*Tenebrio molitor*)

Yunyun Chen,[a] Carlos Sanchez,[b] Yuan Yue,[a] Jorge M. González,[c] Dilworth Y. Parkinson[d] and Hong Liang[a,b]*

[a]Materials Science and Engineering, Texas A&M University, MS 3123, College Station, TX 77843-3123, USA, [b]Mechanical Engineering, Texas A&M University, MS 3123, College Station, TX 77843-3123, USA, [c]Department of Plant Science, California State University, Fresno, CA 93740, USA, and [d]Advanced Light Source, Lawrence Berkeley National Laboratory, Berkeley, CA 94720, USA. *Correspondence e-mail: hliang@tamu.edu

Received 6 January 2016
Accepted 18 June 2016

Edited by A. Momose, Tohoku University, Japan

Keywords: synchrotron X-ray micro-tomography; *K*-edge subtraction; yttrium oxide nanoparticles; mealworms; particle distribution.

Supporting information: this article has supporting information at journals.iucr.org/s

Nanomaterials are being used in medicine, manufacturing and consumer products, but their effects on organisms and the environment are not well understood because of the difficulty in detecting them. Here dual-energy X-ray *K*-edge subtraction was used to track two-dimensional yttrium oxide nanoparticles (which can be found in such household objects as color televisions) in adult mealworms (*Tenebrio molitor*). The insects ingested nanoparticle-infused feed for different time periods, up to 24 h, and the nanoparticles could then be identified at several locations in the insects' head, thorax and abdomen, mostly within the digestive tract. In time, all particles were excreted.

1. Introduction

With advancements in the synthesis and characterization of nanoparticles, their use is expanding, and it is increasingly important to understand their risks and consequences to health and the environment. Engineered nanoparticles (ENPs) containing yttrium oxide (Y_2O_3) have been widely used in electronics (they provide the red color in household televisions) as well as in optical and biological applications (He *et al.*, 2013; Bai *et al.*, 2007; Li *et al.*, 2014), and its wide use means that there is concern about its uptake by plants or insects, and subsequent accumulation and bio-magnification (Judy *et al.*, 2011; Chen *et al.*, 2016). A few studies on the health and environmental impact of cerium oxide (CeO_2) (Zhang *et al.*, 2011; Conway *et al.*, 2014) ENPs have been carried out, but little has been done on other rare-earth ENPs, including yttria, a commonly used air-stable nanomaterial. In this work, we present a study of the uptake of two-dimensional yttria nanoparticles (NPs) in insects. The two-dimension particles were selected because their expanded dimension promotes better detection.

Detection of ENPs in organisms and the environment is a challenge. Current modalities that have been used for detection include optical (Holbrook *et al.*, 2008), magnetic resonance imaging (MRI) (Xia *et al.*, 2011), positron emission tomography (PET) (Sun *et al.*, 2011), ultrasound (Zhang *et al.*, 2015) and X-ray computed tomography (CT) (Walton *et al.*, 2015). Optical imaging has been reported for studies of molecular structure (Pysz *et al.*, 2010; Baker, 2010). Techniques such as MRI and PET can provide whole-body information, but have limitations on their resolution and contrast

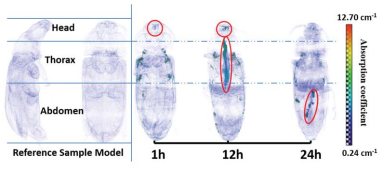

that make it difficult to detect many ENPs (Thorp-Greenwood & Coogan, 2011). Ultrasound has low image contrast and also has limited contrast for ENPs (Zha *et al.*, 2013). X-ray CT has been used to detect ENPs in tissue with high resolution and deep penetration (Kherlopian *et al.*, 2008); dual-energy scanning can take this capability one step further, allowing confirmation of the chemical identity of different species (Cnudde & Boone, 2013; Midgley & Schleich, 2015). In the present research, we have used synchrotron X-ray micro-tomography to characterize the movement of nanoparticles inside insects, including dual-energy *K*-edge subtraction, to track two-dimensional yttria ENPs within mealworms, and we are able to visualize the ENPs and insect in three dimensions (3D).

We have used mealworm beetles (*Tenebrio molitor*; Coleoptera: Tenebrionidae) as a model system in this work because of their relatively large size and ease of rearing and handling (Panagiotakopulu, 2001; Ramos-Elorduy *et al.*, 2002; Finke & Winn, 2004).

2. Methods and characterization

2.1. Synthesis and characterization of yttria NPs

Yttria NPs were synthesized *via* a hydrothermal method. 5.94 mmol Y_2O_3 and 0.02 mmol MgO powders were dissolved in 250 ml HNO_3 solution (2.8 wt%) at 60°C to obtain a transparent solution; then 0.06 mmol $Er(NO_3)_3{\cdot}5H_2O$ and 0.06 mmol $Yb(NO_3)_3{\cdot}5H_2O$ were added. The pH was adjusted to 10.5 by adding 3 *M* KOH solution, at which point white floccules appeared. The resulting 900 ml turbid solution was transferred to a 2 l pressure vessel and heated at 200°C for 12 h. After cooling to room temperature, the precipitate was obtained by centrifugation, and washed by DI water. The final Y-based NPs were obtained by drying the precipitate at 60°C, followed by heating to 1000°C for 3 h in air.

2.2. Yttria NPs exposure and fed-mealworm samples

Yttria NPs were mixed with distilled water followed by mixing with honey water (10% honey and 90% distilled water). *Tenebrio molitor* adults (mealworms) had been reared inside polystyrene boxes with no lids, containing a medium that consisted of crushed wheat and oats, to which a couple of slices (∼4 mm-thick) of a medium-sized apple were added every two weeks. The boxes containing the beetles were kept in a regular day/night regime (in Fresno, California, USA) at a controlled temperature of 25°C and 60% relative humidity. Individuals intended for experiments were selected randomly from fully pigmented beetles (>48 h old). Once the adult mealworms were taken from the general rearing culture to be tested, they were left with no food for five days in a 10 × 15 × 15 cm polystyrene box, with no lid and walls covered with fluon (liquid Teflon). On the sixth day, a quarter of the group (reference sample) was fed with honey water (10% honey) and then taken out and fixed with Kahle's fixative (which allows for a good fixation of the internal tissues and organs of the insect). The remaining mealworms inside the experimental box were then provided with honey water (10% honey) + NPs *ad libitum*. One-quarter of the group was removed after 1 h of feeding, another quarter after 12 h, and the remaining group after 24 h. Each insect was fixed with Kahle's fixative upon extraction from the polystyrene box.

2.3. Micro-tomography

The synchrotron X-ray micro-tomography experiments were conducted at Advanced Light Source (ALS) beamline 8.3.2, Lawrence Berkeley National Laboratory, USA. Imaging energies of 17.3 keV and 16.7 keV were selected, straddling the yttrium *K*-edge energy. Radiographs were acquired, with 512 projections over 180° rotation. Using a LuAG scintillator, pco.Edge scientific CMOS camera and 2× optical lens yielded a pixel size of 0.00329 mm. The exposure time for scanning specimens was 200 ms. The datasets were reconstructed by using a Fourier method implemented in the commercial *Octopus* package. The *K*-edge subtracted datasets were obtained by subtraction of the 16.7 keV reconstructed 32-bit images from the 17.3 keV images. 3D visualization of the distribution of NPs in the mealworms was performed with the *Avizo* software package (FEI).

2.4. Image segmentation

Straddling the Y *K*-edge (17.0 keV), from 16.7 keV to 17.3 keV, Y sees a sharp (five times) increase in its X-ray attenuation coefficient, whereas other elements have very slight decreases in their attenuation coefficients over this range. The location of yttria can be unambiguously identified by subtracting the reconstructed 3D images collected at 16.7 keV from those collected at 17.3 keV (Fig. 1). This is known as the dual-energy *K*-edge subtraction technique. The grayscale value of the reconstructed transverse slices represents the absorption coefficient (units: cm^{-1}). The 17.3 keV dataset and *K*-edge subtracted dataset were used to segment (digitally label) the NPs within mealworms. First, a threshold was set for the 17.3 keV data set, and all values above the threshold were labeled as candidate NPs with the NP areas set to 1 and non-labelled areas to 0. The segmented binary image was multiplied by the *K*-edge subtracted dataset. The resulting data set was again subjected to a threshold, yielding the final map of NPs (as displayed in Fig. 4). This approach successfully allowed identification of NPs, while excluding regions of sample motion or shrinkage (which show up as bright regions in the *K*-edge subtracted dataset) from being identified as NPs.

3. Results and discussion

3.1. Tomographic observation

Because of the higher attenuation coefficient above the *K*-edge, Y_2O_3 NPs appear much brighter (higher grayscale value) at 17.3 keV than at 16.7 keV (Figs. 1*a*, 1*b*); identical brightness and contrast settings are used in these two panels, to allow fair comparison. We also show the *K*-edge subtracted image at this position in the sample (Fig. 1*c*). One source of potential error in this method is sample motion between the

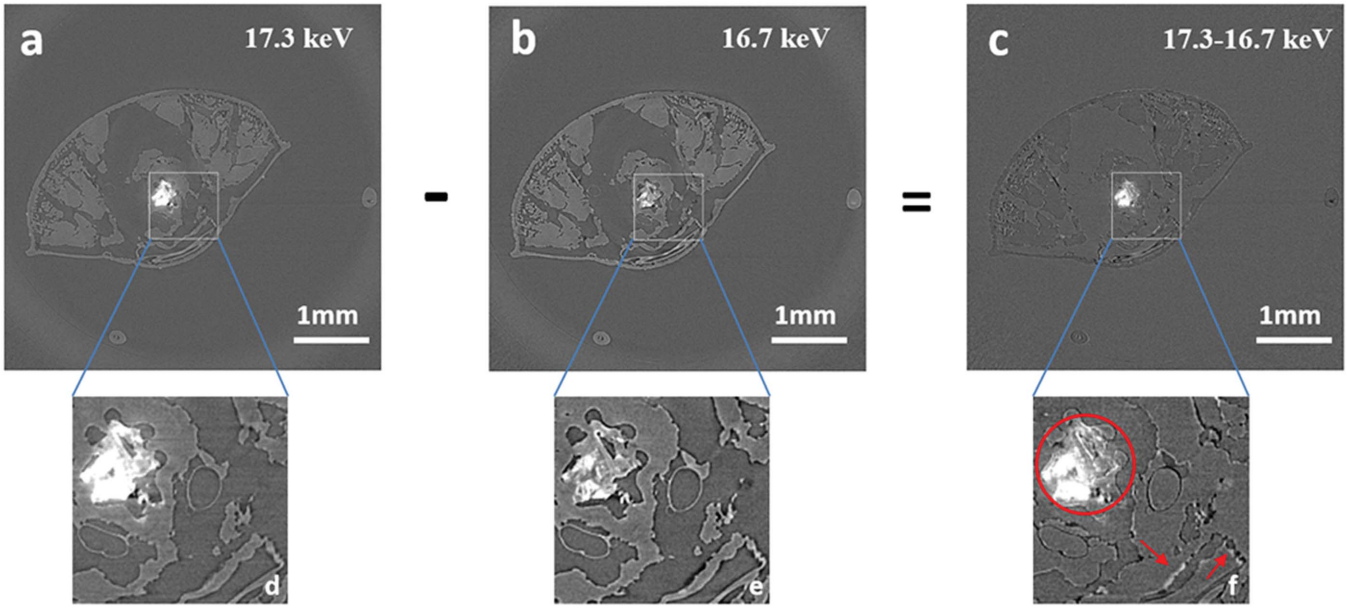

Figure 1
Identification and localization of yttria NPs. (*a*) One reconstructed digital slice from 12 h-fed mealworm sample scanned using 17.3 keV X-rays, above the yttrium *K*-edge energy. (*b*) The same slice scanned at 16.7 keV, below the Y *K*-edge. (*c*) *K*-edge subtraction image, obtained by the subtraction of the 16.7 from 17.3 keV slice. (*d*, *e*, *f*) Enlarged areas showing aggregates of yttria NPs (circled) and the image artifacts due to sample motion or tissue shrinkage that can be excluded from identification as NPs (arrows).

above- and below-edge scans. The area marked with a circle in Fig. 1(*f*) shows the localization of Y_2O_3 NPs and also, in the areas marked with arrows, regions of increased brightness which were actually caused by shrinkage of biological tissue between or during the scans (Fig. 1*f*). Problems due to sample motion such as those marked by these arrows generally have regions of increased brightness adjacent to regions of increased darkness, making it possible to avoid these regions during analysis; additionally, the pixel values in these regions in the difference image are substantially less than in the regions with NPs.

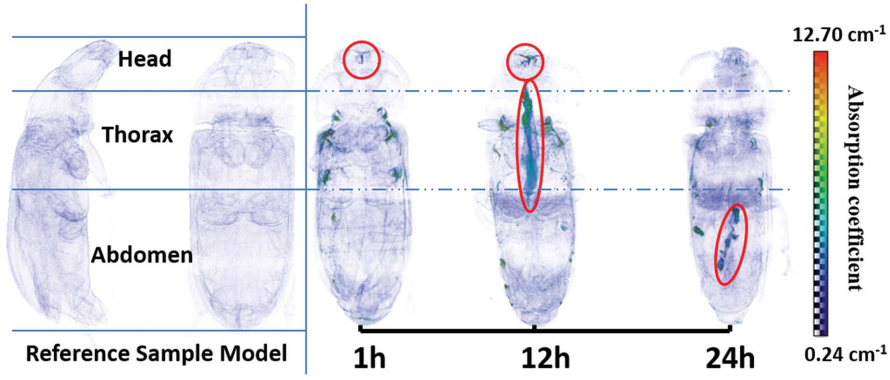

Figure 2
Translocation of NPs within mealworms with extended feeding time. 3D visualization of samples, using the (above/below/difference) data. The most concentrated distribution of NPs inside the mealworms is labeled with red circles. Regions of apparently high NP concentration that are not circled are on the outside surface of the mealworm, spread by their grooming actions.

3.2. Pathways of nanoparticles

The translocation of NPs within mealworms is evident by comparing the 3D visualization of the insects that experienced each of the four different NP feeding times (0, 1, 12 and 24 h) (Fig. 2). To better understand how the nanoparticles aggregate and move inside the insect, we studied two-dimensional digital slices through the reconstructed 3D volume, with contrast inverted so that NPs are in the darker (more black) regions (Fig. 3). The reference sample shows no NPs or other highly X-ray attenuating features. For mealworms that fed on NPs, the NPs can be observed moving from the mouthparts (head) to the abdomen (Fig. 2). After 1 h, we can clearly see that the NPs were mainly located passing the mouthparts inside the head and into the foregut (Fig. 2, 3*a*). Fig. 3(*b*) shows that the NPs were swallowed into the buccal cavity (black mark) and flowed into the pharynx (red). The transverse slice shows the NPs located at the pharynx (Fig. 3*c*, red). After passing the pharynx, the NPs moved to the oesophagus (Fig. 3*d*, purple).

After 12 h, even though the NPs can be seen at the head (mealworms were feeding *ad libitum*), they are additionally moving through the digestive system and can be seen in the thorax and entering the abdomen (Fig. 2). Fig. 3(*e*) presents the 12 h fed sample with NPs accumulated in the thoracic region. The NPs were passing through but accumulated along the walls of the pharynx and the oesophagus. Passing the oesophagus, the NPs went into the crop, as marked by the yellow circles in Figs. 3(*f*) and 3(*g*). The buccal cavity,

pharynx, oesophagus and crop are all part of the foregut, which is ectodermal in origin (Snodgrass, 1935), and they do not allow exchange of nutrients through their walls into the coelom (the main body cavity surrounding and containing the digestive tract and other organs). This is the reason why the NPs were observed passing through or accumulating inside the digestive tract, but not moving into the coelom in the head. However, after the NPs migrated into the midgut, where most digestion and absorption of nutrients takes place in insects, some NPs entered the coelom through the midgut wall (Fig. 3*h*, blue).

After 24 h, the NPs have continued moving through the digestive system and are located in the abdomen of the mealworm (Fig. 2). Fig. 3(*i*) shows the NPs accumulated along part of the midgut and in the proctodeum (hindgut or terminal portion of the insect digestive system) in the 24 h-fed mealworm. The blue circles in transverse slices show the NPs localized in the midgut (Figs. 3*j* and 3*k*). With the exchanging of the nutrients allowed in the midgut, NPs were absorbed, accumulated and encapsulated inside the coelom (Figs. 3*j* and 3*k*, white). Fig. 3(*l*) shows the NPs inside the anterior intestine, which is part of the hindgut. The hindgut is also ectodermal in origin and does not allow nutrient exchange. All solid materials that migrated to the proctodeum would be eventually excreted through the anus.

In addition to NPs inside the mealworm beetles, we also found NPs adhering to their outside surface. We attribute this to mealworm grooming; during and after eating they use their legs to 'clean' the mouthparts, the head and the body, thus spreading NPs over their exterior surface. NPs adhering to the outside surface of the mealworm body are marked with green markers in Fig. 3.

We identify and visualize the accumulation of NPs in specific organs in 3D in Fig. 4. When NPs have moved inside

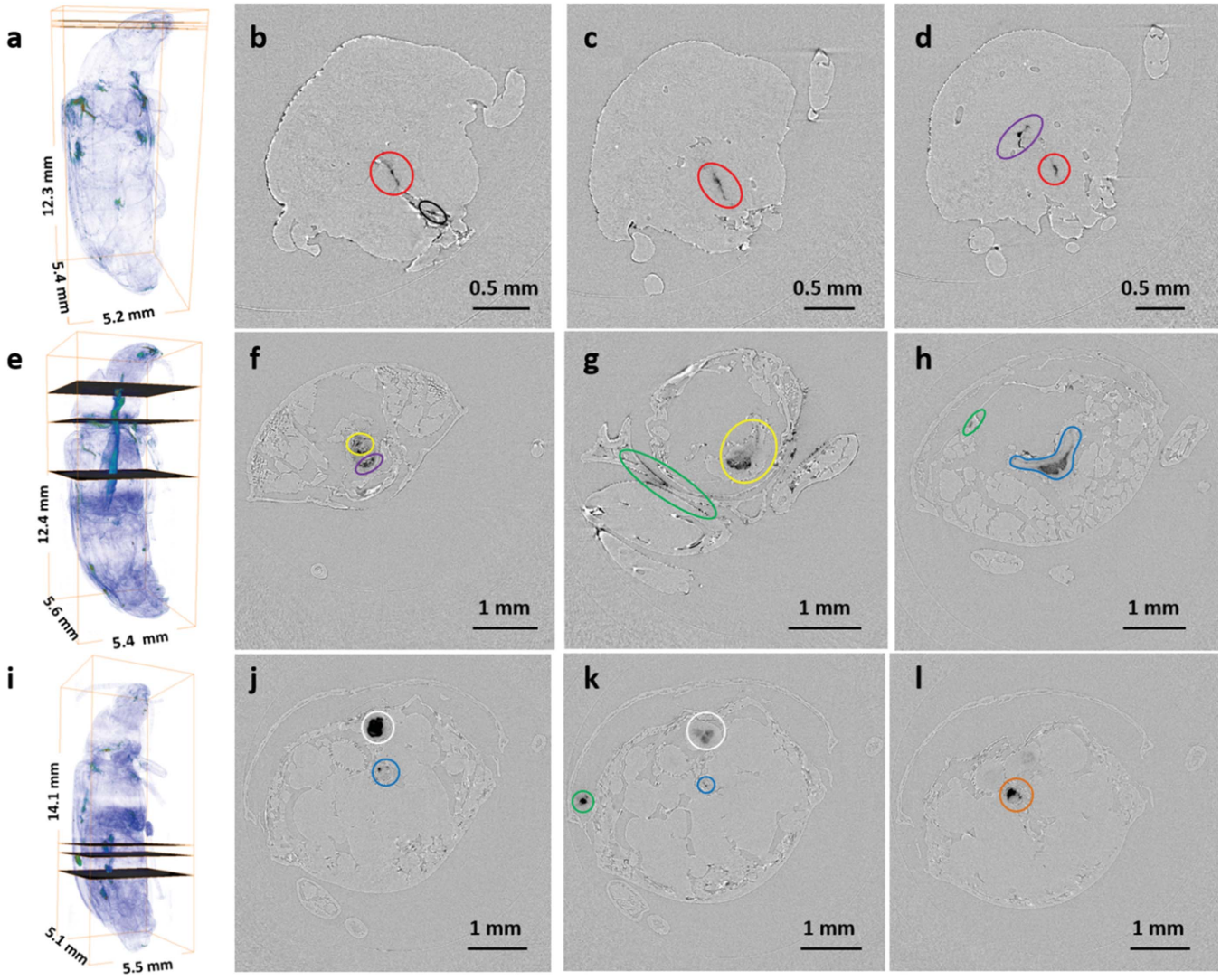

Figure 3
Localization of NPs inside the digestive system of the mealworms. (*a*, *e*, *i*) 3D visualizations indicating the locations of three slices which are displayed to the right of those panels; (*a*) head segment of 1 h-fed mealworm sample, (*e*) thorax segment of 12 h-fed mealworm sample, (*i*) abdomen segment of 24 h-fed mealworm sample. The dark (nearly black) regions within the colored circles are identified as NPs; other dark areas result from the shift of biological tissue between the two X-ray scans. Colored circles correspond to: black, buccal cavity; red, pharynx; purple, oesophagus; yellow, crop; green, on surface; blue, midgut; white, encapsulated NPs inside coelom; orange, anterior intestine.

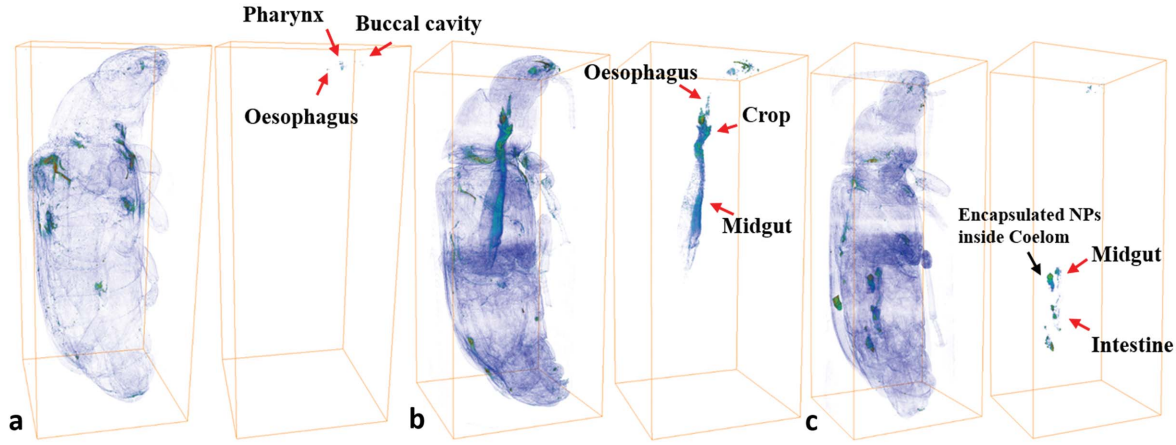

Figure 4
Distribution of NPs within mealworms organs. The accumulated NPs inside the (*a*) 1 h-, (*b*) 12 h- and (*c*) 24 h-fed mealworm.

the coelom, a hemocyte-mediated reaction from the hemolymph encapsulates the particles, a defense response system that we have reported earlier in other insects (Rocha *et al.*, 2011). Once the NPs are encapsulated in the coelom, they are not excreted through the anus, and the probability of NPs accumulation and subsequent translocation to higher trophic animals increases.

4. Conclusions

We used dual-energy *K*-edge subtraction to track two-dimensional Y_2O_3 NPs in mealworms. We clearly identified the Y_2O_3 NP accumulation locations as they passed through the mealworm digestive system, and, importantly, we also found that NPs passed into and accumulated in the coelom. Accumulation of NPs at the coelom could result in their translocation to higher trophic level animals and potentially lead to toxicity and biomagnification. Our success in this work also indicates the feasibility of this method for studying nanoparticles in other organisms. Future research will focus on the effects of nanoparticles on the behavior of mealworms.

See also the supporting information for transmission electron microscope images of the NPs.

Acknowledgements

YYC was partially sponsored by an ALS fellowship. JMG was supported by the Provost's Assigned Time for Research (Summer 2015) and California State University Fresno, Research, Scholarship and Creative proposal Awarded (2014–2015). The Advanced Light Source is supported by the Director, Office of Science, Office of Basic Energy Sciences, of the US Department of Energy under Contract No. DE-AC02-05CH11231. YYC, CS, YY and JMG conducted the experiments; YYC and JMG analyzed the data; DYP and HL designed the experiments; YYC, JMG, DYP and HL wrote the paper. All authors reviewed the manuscript. Authors state no competing financial interests.

References

Bai, X., Song, H. W., Pan, G. H., Lei, Y. Q., Wang, T., Ren, X. G., Lu, S. Z., Dong, B., Dai, Q. L. & Fan, L. (2007). *J. Phys. Chem. C*, **111**, 13611–13617.
Baker, M. (2010). *Nature (London)*, **463**, 977–980.
Chen, Y., Sanchez, C., Yue, Y., Almeida, M. de, González, J. M., Parkinson, D. Y. & Liang, H. (2016). *J. Nanobiotechnol.* **14**, 23.
Cnudde, V. & Boone, M. N. (2013). *Earth Sci. Rev.* **123**, 1–17.
Conway, J. R., Hanna, S. K., Lenihan, H. S. & Keller, A. A. (2014). *Environ. Sci. Technol.* **48**, 1517–1524.
Finke, M. & Winn, D. (2004). *J. Wildl. Rehabil.* **27**, 14–27.
He, X. L., Zhou, Y. & Liang, H. (2013). *J. Mater. Chem. C.* **1**, 6829–6834.
Holbrook, R. D., Murphy, K. E., Morrow, J. B. & Cole, K. D. (2008). *Nat. Nano*, **3**, 352–355.
Judy, J. D., Unrine, J. M. & Bertsch, P. M. (2011). *Environ. Sci. Technol.* **45**, 776–781.
Kherlopian, A. R., Song, T., Duan, Q., Neimark, M. A., Po, M. J., Gohagan, J. K. & Laine, A. F. (2008). *BMC Syst. Biol.* **2**, 74.
Li, R., Ji, Z., Chang, C. H., Dunphy, D. R., Cai, X., Meng, H., Zhang, H., Sun, B., Wang, X., Dong, J., Lin, S., Wang, M., Liao, Y. P., Brinker, C. J., Nel, A. & Xia, T. (2014). *ACS Nano*, **8**, 1771–1783.
Midgley, S. & Schleich, N. (2015). *J. Synchrotron Rad.* **22**, 807–818.
Panagiotakopulu, E. (2001). *J. Archaeol. Sci.* **28**, 1235–1246.
Pysz, M. A., Gambhir, S. S. & Willmann, J. K. (2010). *Clin. Radiol.* **65**, 500–516.
Ramos-Elorduy, J., González, E. A., Hernández, A. R. & Pino, J. M. (2002). *J. Econ. Entomol.* **95**, 214–220.
Rocha, A., Zhou, Y., Kundu, S., Gonzalez, J. M., Vinson, S. B. & Liang, H. (2011). *J. Nanobiotechnology*, **9**, 5.
Snodgrass, R. E. (1935). *Principles of Insect Morphology*. New York: McGraw-Hill.
Sun, Y., Yu, M., Liang, S., Zhang, Y., Li, C., Mou, T., Yang, W., Zhang, X., Li, B., Huang, C. & Li, F. (2011). *Biomaterials*, **32**, 2999–3007.
Thorp-Greenwood, F. L. & Coogan, M. P. (2011). *Dalton Trans.* **40**, 6129–6143.
Walton, L. A., Bradley, R. S., Withers, P. J., Newton, V. L., Watson, R. E. B., Austin, C. & Sherratt, M. J. (2015). *Sci. Rep.* **5**, 10074.
Xia, A., Gao, Y., Zhou, J., Li, C., Yang, T., Wu, D., Wu, L. & Li, F. (2011). *Biomaterials*, **32**, 7200–7208.
Zha, Z. B., Wang, S. M., Zhang, S. H., Qu, E. Z., Ke, H. T., Wang, J. R. & Dai, Z. F. (2013). *Nanoscale*, **5**, 3216–3219.
Zhang, H. F., He, X. A., Zhang, Z. Y., Zhang, P., Li, Y. Y., Ma, Y. H., Kuang, Y. S., Zhao, Y. L. & Chai, Z. F. (2011). *Environ. Sci. Technol.* **45**, 3725–3730.
Zhang, K., Chen, H., Guo, X., Zhang, D., Zheng, Y., Zheng, H. & Shi, J. (2015). *Sci. Rep.* **5**, 8766.